A Comparative Study of Three Different Chemical Vapor Deposition (CVD) Techniques of Carbon Nanotube Growth on Diamond Films

Betty T. Quinton[a,b], Paul N. Barnes[c], Chakrapani V. Varanasi[e], Jack Burke[d], Bang-Hung Tsao[d], and Sharmila M. Mukhopadhyay[b]

a. Air Force Research Laboratory (AFRL), WPAFB, OH 45433, USA

b. Wright State University, Dayton, OH 45420, USA

c. Army Research Laboratory, Adelphi, MD 20783, USA

d. University of Dayton Research Institute (UDRI), Dayton, OH 45469, USA

e. Army Research Office, Research Triangle Park, NC 27709, USA

Abstract:

Successful attachment of carbon nanotubes (CNTs) on diamond substrates can lead to unique power devices with superior thermal and electronic properties. However, there is very little investigation on the diamond-CNT structures, and on suitability of different growth methods. This study addresses that gap by investigating three potential Chemical Vapor Deposition (CVD) techniques for growing CNTs on diamond, and comparing their effectiveness. The diamond substrate is a commercially grown polycrystalline film. The CNT growth techniques that have been compared are as follows: thermal CVD (T-CVD), microwave plasma enhanced CVD (MPE-CVD), and floating catalyst thermal CVD (FCT-CVD). The first two approaches require pre-deposition of catalyst sources prior to CNT growth, while the last method feeds the catalyst continuously during the CNT growth process. Scanning Electron Microscopy (SEM) and high resolution Transmission Electron Microscopy (TEM) have been used to analyze the morphology and topology of the CNT structures. Raman spectroscopy was used to assess the quality of the

Report Documentation Page

Form Approved
OMB No. 0704-0188

1. REPORT DATE	2. REPORT TYPE	3. DATES COVERED
2013		**00-00-2013 to 00-00-2013**

4. TITLE AND SUBTITLE	5a. CONTRACT NUMBER
A Comparative Study of Three Different Chemical Vapor Deposition (CVD) Techniques of Carbon Nanotube Growth on Diamond Films	5b. GRANT NUMBER
	5c. PROGRAM ELEMENT NUMBER
6. AUTHOR(S)	5d. PROJECT NUMBER
	5e. TASK NUMBER
	5f. WORK UNIT NUMBER
7. PERFORMING ORGANIZATION NAME(S) AND ADDRESS(ES) **Air Force Research Laboratory,WPAFB,OH,45433**	8. PERFORMING ORGANIZATION REPORT NUMBER
9. SPONSORING/MONITORING AGENCY NAME(S) AND ADDRESS(ES)	10. SPONSOR/MONITOR'S ACRONYM(S)
	11. SPONSOR/MONITOR'S REPORT NUMBER(S)

12. DISTRIBUTION/AVAILABILITY STATEMENT
Approved for public release; distribution unlimited

13. SUPPLEMENTARY NOTES
Preprint Journal of Nanomaterials, 2013

14. ABSTRACT

15. SUBJECT TERMS

16. SECURITY CLASSIFICATION OF:			17. LIMITATION OF ABSTRACT	18. NUMBER OF PAGES	19a. NAME OF RESPONSIBLE PERSON
a. REPORT	b. ABSTRACT	c. THIS PAGE			
unclassified	**unclassified**	**unclassified**	**Same as Report (SAR)**	**23**	

grown CNTs by determining the D-peak to G-peak intensity ratios. Sonication tests were performed to provide qualitative comparisons of the durability of the CNT forests. T-CVD provides the largest diameter tubes with catalysts residing mainly at the CNTs/diamond interface, the MPE-CVD provides non-uniform defective CNTs, and the FCT-CVD provides the smallest diameter CNTs with catalyst particles imbedded throughout the length of the nanotubes. The three different CNT growth methods have been discussed in light of our current understanding of CNT growth mechanisms on the synthetically grown polycrystalline diamond film.

1. Introduction:

Carbon nanotubes (CNTs) are lightweight materials that express superior mechanical, electrical and thermal properties [1–4]. Diamond films are well known for their hardness and scratch resistance combined with excellent thermal conductivity [5,6]. Successful CNT growth on a diamond substrate creates a unique all-carbon structure that can be beneficial for advanced power and electronic applications. Various methods such as Chemical Vapor Deposition (CVD), laser ablation, thermal evaporation, arc-discharge, and glow-discharge have been used to grow CNTs on different surfaces [7–9] including diamond substrates and nanoparticles [9–11]. Among these methods, CVD is perhaps the most promising and scalable approach for future power and electronic devices.

There are many different varieties of CVD used to grow CNTs. The variations depend on power sources, type of catalyst deposition, gas composition, and operating temperatures. In addition to variations of the CVD process, CNT growth is expected to depend significantly on the chemistry, morphology, and activity of the substrate. Catalyst and substrate interactions can create

differences in root growth or tip growth mechanisms, size distribution as well as defects in CNTs growth [12–14].

Several CVD approaches have been investigated and documented on common electronic substrates such as silicon, but no work seems to have been reported on specialty substrates such as diamond. It is desirable to test the applicability of these techniques on diamond substrates and compare the CNTs obtained from different CVD growth techniques. This would enable future device manufacturers to select the most appropriate technique for a specific application. This study compares three types of CVD techniques believed to be the most probable candidate techniques to be scaled up and utilized for future power devices. They all utilize transition metal catalysts that can readily form metastable carbides needed for CNT growth on any substrate [15–17]. The three CVD approaches selected were: thermal CVD (T-CVD) with pre-sputtered metal catalyst, microwave plasma enhanced CVD (MPE-CVD) with pre-sputtered metal catalyst and floating catalyst thermal CVD (FCT-CVD) with xylene and ferrocene liquid mixture without any prior catalyst deposition. T-CVD is a low cost system that can easily be set up to grow CNTs. In comparison to arc discharge, T-CVD operates at a lower temperature which increases the range of substrate material selections. However, the resulting CNTs structure may be defective compared to arc-discharge or laser ablation [18]. MPE-CVD is very suitable for large surface CNT production, and can grow CNTs at even lower temperatures than T-CVD [19]. Both these techniques involve pre-deposition of catalyst on the substrate. The FCT-CVD introduces carbon source and catalyst simultaneously on the substrate as a gas mixture. This approach cuts out the first step of catalyst deposition giving it an advantage for future scaling-up. However, it coats everything in the growth chamber, and may be problematic when select area growth is required [20].

The CNT forests grown have been investigated in detail and each sample has been analyzed using a scanning electron microscope (SEM), transmission electron microscope (TEM), Raman spectroscopy, and energy dispersive x-ray spectroscopy (EDS) to fully characterize the structures.

2. Experimental Methods:

2.1 Sample Preparation:

Polished free standing diamond substrates grown by a CVD technique were purchased from SP^3 Diamond Technologies Inc. The substrate measurements were 5 x 5 mm^2, with a 400 µm thickness. The surface roughness was determined to be 5 nm as measured by an atomic force microscope. Three CVD based CNT growth techniques have been investigated: (i) T-CVD, (ii) MPE-CVD, and (iii) FCT-CVD. The first two techniques involved pre-deposition of seed catalysts prior to CNT growth, and were optimized first on an electronic grade silicon substrate with a layer of thermal silicon dioxide layer on the surface. The last one had the catalyst source combined with the carbon source in the feeder gas, and had been optimized earlier on graphitic carbon substrates.

Due to limited quantities of CVD diamond substrates, each of the growth methods described below were first tested and optimized using other standard substrates before deposition on the diamond. While it is recognized that optimization of parameters on identical diamond substrate would be ideal, the large number of diamond substrates necessary for such an undertaking was not available. It was, however, verified that the growth conditions on standard substrates were repeatable on other available substrates. As for growth parameters of CNTs on diamond available in the literature the values reported for T-CVD and MPE-CVD were found to be very

comparable to ones deduced in-house on standard substrates [10,21]. There is no reported growth on CNTs on diamond substrate using the FCT-CVD method. However, this technique involves pre-coating the substrate with a plasma-enhanced oxide layer, which is expected to make the CNT growth more independent of the underlying substrate. Additional optimization and refinement on specific diamond substrates may be performed in the future as more varieties of diamond substrates become available in larger quantities. At the current time, Raman spectroscopy for the T-CVD method is used as an indicator of CNT quality, and the D-peak to G-peak intensity ratios from CNTs obtained on all samples were more than satisfactory. Successful and repeatable experiments from earlier research indicated that the best CNT forests were obtained by using T-CVD and MPE-CVD growth process with nickel and iron catalysts, respectively. For the FCT-CVD approach, ferrocene is used as an iron source to promote CNT growth. Based on these repeatable results, the CNT growth parameters were used to grow CNTs on the diamond films.

2.2 T-CVD method:

Polished free standing CVD diamond substrates were cleaned in an ultrasonic acetone bath for 5 minutes followed by 5 minutes in ultrasonic isopropanol bath. After cleaning, the samples were placed into a radio frequency (RF) sputtering system loaded with a 99.999% pure nickel target. The sputtering system uses RF power to create a plasma plume that deposits material from the target to the substrate surface. The substrate was first sputtered with a 10 nm thin film of nickel in a sputter chamber. Then the nickel-sputtered sample was then placed into a T-CVD furnace. The furnace was heated from room temperature to the growth temperature of 800 $^{\circ}$C in 20 minutes with an Argon/5% Hydrogen (Ar/5%H_2) gas mixture at a flow rate of 300 standard

cubic centimeters per minute (sccm). Upon reaching the growth temperature, the sample was held for 10 minutes to allow the thin nickel film to break up into nanoscale islands. Then 400 sccm of Argon/10% Methane ($Ar/10\%C_2H_2$) was introduced as the carbon feedstock source at the end of the 10 minute heat treatment. The growth process continued for 2 hours followed by a slow cool to room temperature again using a flow of 300 sccm of a ($Ar/5\%H_2$) gas mixture. The entire growth process was performed at a pressure of 90 torr.

2.3 MPE-CVD method:

The same sample cleaning procedures discussed above were followed here. The sputtering process was used again, but with 99.999% pure iron target to form a 10 nm thin film of iron on the CVD diamond samples. The sample was loaded into the MPE-CVD chamber. The furnace was heated from room temperature to 400 $^{\circ}$C with pure hydrogen gas flowing at 150 sccm. Once the temperature reached 400 $^{\circ}$C, a microwave frequency was used on the hydrogen gas to induce hydrogen plasma within the chamber. The sample was held for 5 minutes with the hydrogen plasma at 400 $^{\circ}$C to allow iron island formation. After 5 minutes of annealing in plasma, the temperature was increased to the 650 $^{\circ}$C growth temperature, followed by the introduction of 15 sccm of methane gas as a carbon source. Methane gas was allowed to flow for 5 minutes for growth to take place. After that, hydrogen plasma was reduced to hydrogen gas and the methane gas was shut off. The heating unit was turned off to allow the system to cool naturally.

2.4 FCT-CVD method:

The free standing CVD diamond samples were treated with microwave plasma containing dimethyl sulfoxide (DMSO) to deposit a thin film of silica, 100 nm in thickness, onto the CVD

diamond substrate. Note that there is a correlation between silica thickness and the quality of CNTs and that this silica layer is required in order for CNTs to grow using FCT-CVD methods [22,23]. The FCT-CVD system is a two stage furnace with Ar gas flowing at 600 sccm and hydrogen gas flowing at 45 sccm. The low temperature furnace is kept at 250 $^{\circ}$C while the high temperature furnace is ramped up to the growth temperature of 750 $^{\circ}$C. Ferrocene was dissolved into xylene solvent in a 0.008: 1 molar volume ratio. The xylene/ferrocene liquid mixture serves as carbon feed stock as well as an iron catalytic particle source carrier. During growth, xylene/ferrocene was introduced at a flow rate of 3 ml/hr via a syringe pump. The growth time was 20 minutes followed by cool down with 600 sccm of Ar gas. Details of silica treatment as well as the CNT growth parameters can be found in earlier publications [24].

2.5 Characterization:

The resulting samples were characterized using a FEI Sirion high resolution SEM for analysis of carpet surface and nanotube morphology. Cross sectional views of the interfaces are needed to understand how catalyst particles play a role during CNT growth. A thin TEM foil of the cross section of interest was made using a DB235 FEI focus ion beam. To protect CNTs from the gallium ion etching, a layer of platinum cap was sputtered on top of the CNT before the trenching process began for a lift out sample. The resulting foil was attached to a molybdenum TEM grid for final thinning until a transparent foil was formed. The TEM foil was first analyzed using a Philips CM200 TEM for general appearances and identifies the different layers that it contains. The foils containing CNTs with both catalyst and substrate intact were then analyzed for elemental compositions by energy dispersive X-ray spectroscopy (EDS) using the FEI Titan 80-300 TEM. In addition to the imaging analysis, Raman spectroscopy analysis was used to

provide a qualitative value for the growth structures of CNTs. It uses the intensity ratio of the disorder peak (D-peak) over the graphite peak (G-peak) to determine this qualitative value [25]. In order to monitor the durability and strength of bonding between CNTs and the diamond substrate, a sonication test was performed on samples made from each growth method. This test uses Bransonic 3210, an ultrasonic cleaner with 40 kHz frequency. The samples were sonicated for 15 minutes while submerged in deionized water. The results from the previous analyses are discussed in the next section.

3. Results & Discussions:

3.1 Initial Catalyst Distribution in pre-seeded samples:

It is well established that the underlying catalysts play a big role in the structure and properties of the resulting CNTs. The three different techniques compared here have two different approaches of introducing the catalyst: T-CVD and MPE-CVD involve pre-deposition of nickel and iron catalysts respectively, while FCT-CVD technique introduces catalyst with the feeder gas during CNT growth. In the first two cases, the morphology of the starting catalyst film could be analyzed prior to CNT growth. For the last case, there is no precursor catalyst film and catalyst morphology can only be seen after the CNT layer is formed, as discussed later.

Figure 1a shows that thermal treatment of the 10 nm nickel film covering the polished diamond surface resulted in nanoislands with average diameters of 53 nm distributed uniformly across the substrate surface. According to Homma, et al. [26] the resulting particle size can be modified and is dependent on the film thickness. A thinner film thickness using the procedure mentioned

above provided a low CNTs growth yield. Because of this, the study uses 10 nm film thicknesses as the testing film thickness.

Figure 1b shows the SEM surface analysis of a sample treated at 400 °C with hydrogen plasma inside the MPE-CVD system for 5 minutes. The image shows that the iron catalyst agglomerated into a continuous uneven film rather than solidified as isolated nanoparticles.

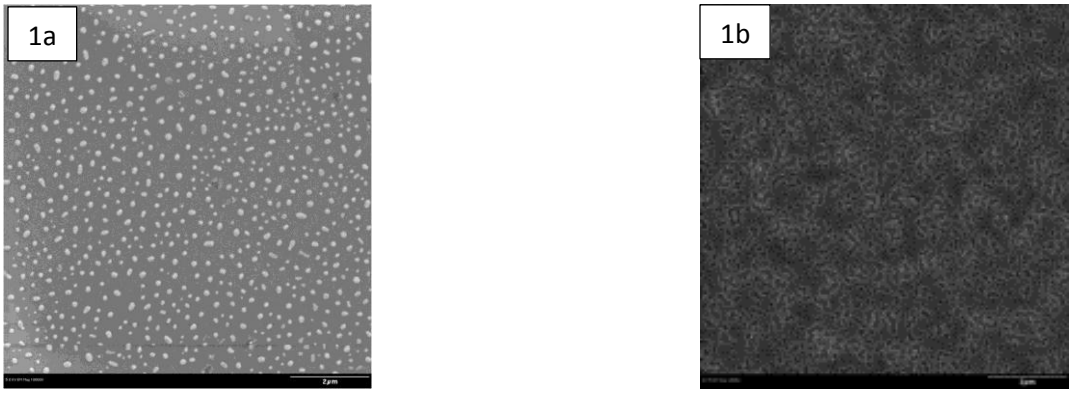

Figure 1a: Ni catalyst after thermal treatment in T-CVD. Figure 1b: Fe catalyst after thermal treatment in MPE-CVD with hydrogen plasma.

3.2 Nanotube Morphology:

Figure 2 shows SEM images of the CNT layer formed on diamond film using the three different techniques. Figure 2a is the image of T-CVD grown CNTs which have an average tube diameter of 61 nm ± 12 nm, with smooth and uniform tubular structure. This correlates well with the uniform size distribution of nickel islands of similar size seen in Figure 1a.

Figure 2b, is a SEM image of MPE-CVD grown CNTs that indicates the CNTs are not uniform and contain various defects, as well as variation in diameters. This may be the result of the seed catalyst layer consisting of irregular shaped particles. The non-uniformity of individual tubes may also be influenced by defects developed during formation. The MPE-CVD method uses

hydrogen plasma that forms a reducing environment within the chamber. Furthermore, as the methane gas is decomposed more hydrogen molecules are being produced. The SEM image taken can be compared to the study done by Behr which indicates that hydrogen can etch CNTs during the growth process. This can create surface defects throughout the growth process [27]. Some studies suggest that exposing growing CNTs to hydrogen-rich environments convert them into diamonds [28, 29]. Figure 2b shows the MPE-CVD CNTs tubes with defects similar to ones reported by Behr after exposure to the hydrogen-rich environment.

Figure 2c, shows image of FCT-CVD grown CNTs. This figure indicates that the CNTs are uniform in diameter and grow as densely entangled forests. These CNTs have average diameters of 12 nm ± 1.8 nm, making them the smallest of the three growth methods. The image also suggests that there are particles residing on the outer surface of the CNTs. This is expected because the xylene/ferrocene mixture provides continuous source of iron particles throughout the entire process, some of which are expected to attach to the growing CNT surface. The diameter of the outer particles can provide an estimate of iron catalyst size, and they are averaging diameter size of 12 nm ± 2.2 nm.

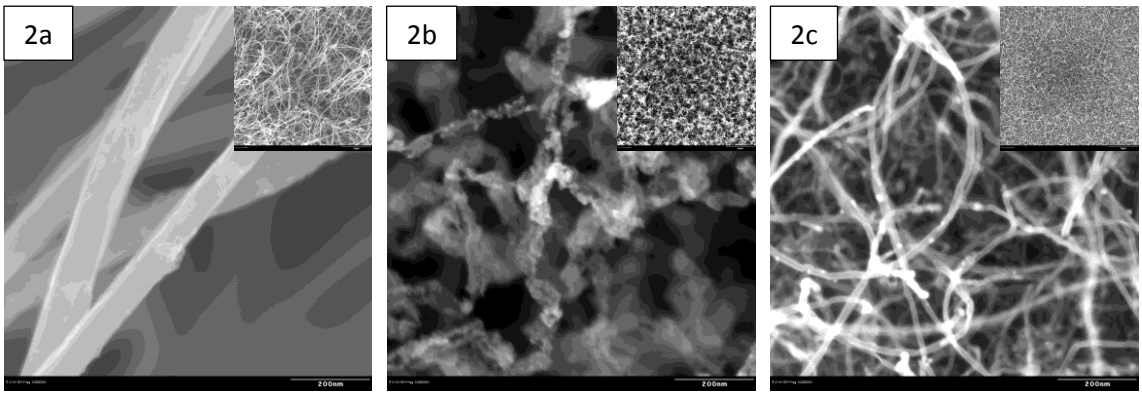

Figure 2a: T - CVD grown CNTs., 2b: MPE - CVD grown CNTs., 2c: FCT - CVD grown CNTs

3.3 Catalyst distribution in the final CNT-covered diamond structure

Figures 3-5 show high resolution TEM images with EDS elemental mapping. Figure 3 indicates that in T-CVD, nickel particles are encapsulated with a layer of carbon, and CNT growth originates from the outer carbon layer. This explains why the average CNT diameter is slightly higher than the average nickel catalyst diameter as shown later. The encapsulated catalyst particle remains anchored at the diamond-CNT interface implying the predominant growth mechanism is root growth. There are a few instances where the catalyst particle moved several nanometers into the CNT length, away from the interface. Growth patterns similar to this indicate a small probability of catalyst lift-off.

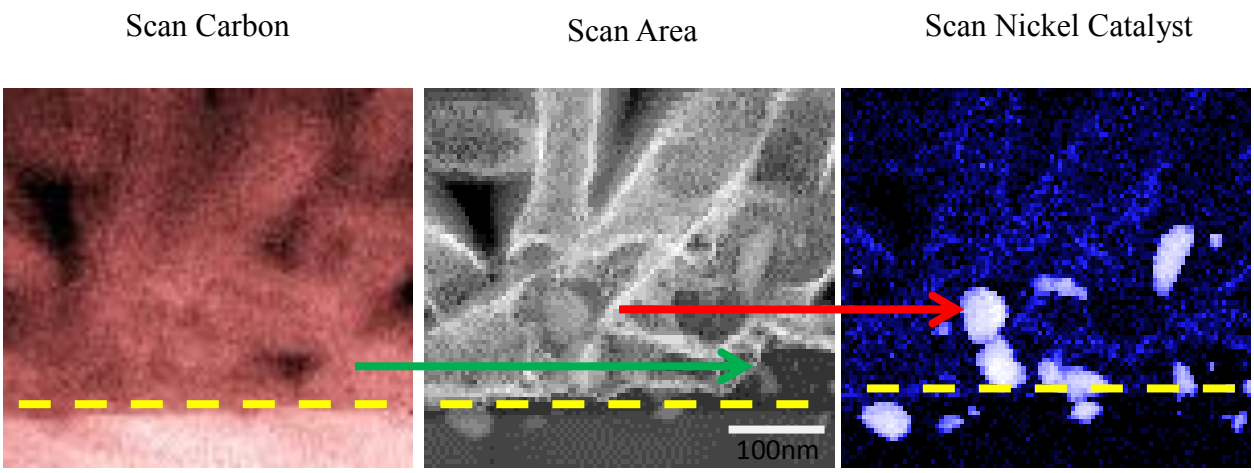

Figure 3: Cross sectional TEM image of T - CVD grown CNTs, the scale bar is 100 nm

Figure 4 shows an energy filtered-transmission electron microscope (EF-TEM) image of an MPE-CVD film. It can be seen that iron particles in this case do not reside along the interface, but rather move easily into the CNT, away from the interface. The mobility of non-anchored catalytic particles at the interface may also contribute to disordered CNT growth.

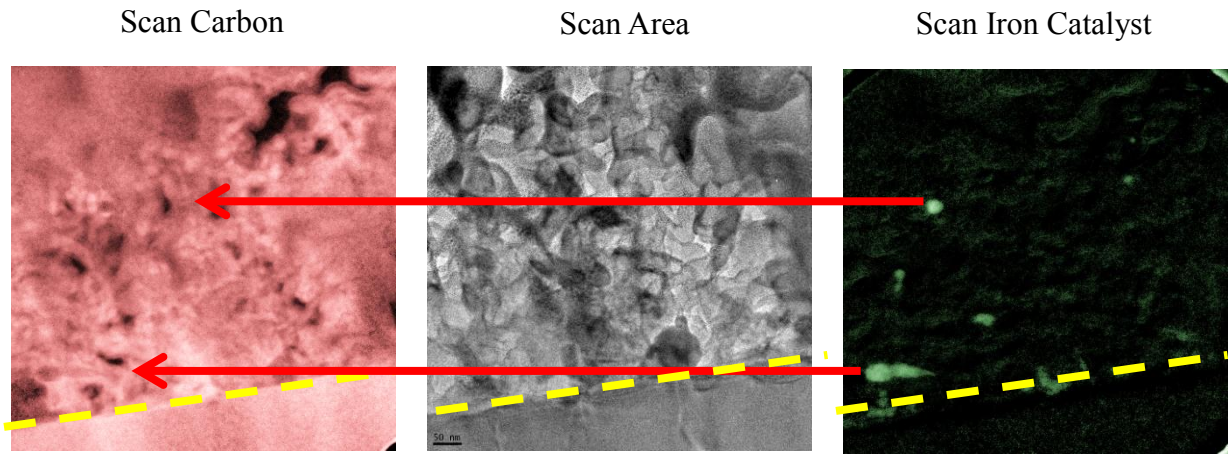

Figure 4: Cross sectional TEM image of MPE-CVD grown CNTs, the scale bar is 50 nm.

As seen in Figure 5, EF-TEM analysis of the FCT-CVD sample indicates a high distribution of iron particles residing at the diamond CNT interface which has the silica functional layer. There are additional iron particles found further away in the CNT forest. This is expected due to the continuous iron particle introduction throughout the CNT growth phase. The large number of iron catalysts at the interface suggests the silica nanolayer keeps them anchored and prevents them from migrating during CNT growth.

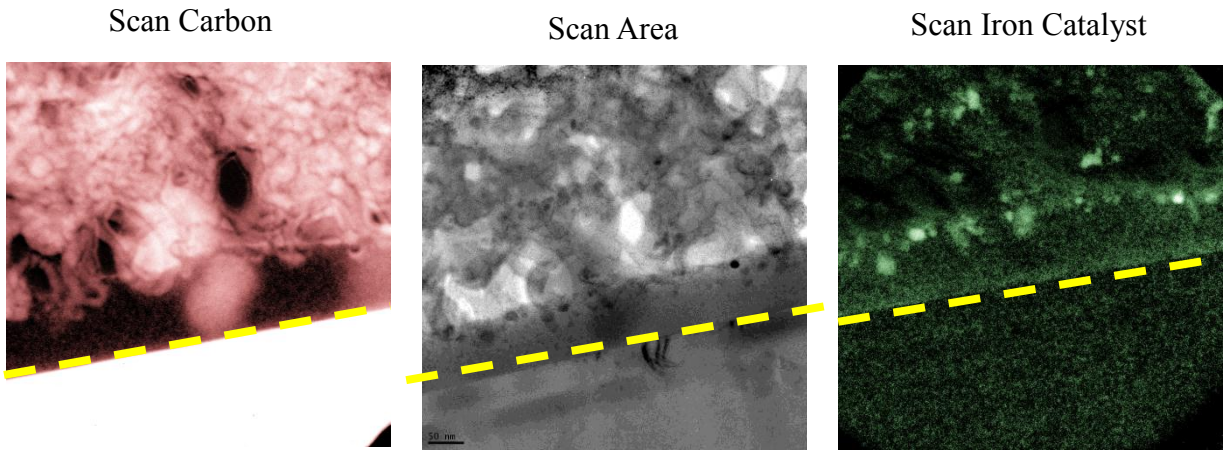

Figure 5: Cross sectional TEM image of FCT -CVD grown CNTs, the scale bar is 50nm.

Figure 6 shows the average particle size distribution taken with ImageJ software. This software provides a qualitative values for the catalyst particle size and tube diameter comparison taken from the resulting TEM images. For T-CVD, the average catalyst particle diameter was measured to be 53 nm ± 16 nm and the average tube diameter was 61nm ± 12 nm. Thus the catalyst diameters measured using TEM images are within the margin of error with the top view images seen by SEM. For MPE-CVD, the average catalyst particle diameter was 21 nm ± 7 nm and the average tube diameter was 40 nm ± 18 nm. For the FCT-CVD method, the average catalyst particle size was 12 nm ± 2 nm and the average tube diameter was 12 nm ± 2 nm. Cross-sectional TEM images provided additional information about particle location and concentration relative to the interface. For T-CVD, the image indicated that catalyst particles are the largest of all growth methods and reside close to the interface. For MPE-CVD, the catalyst particles are distributed away from the interface. This migration may be due to either the fact that they are smaller in size compared to T-CVD samples, or the excess energy provided by the hydrogen plasma or both. For FCT-CVD, the image indicates the majority of the iron particles used as catalysts are anchored along the SiO_2 layer and the iron particles that arrived later reside outside the growing CNTs. The anchoring of smaller nanoparticles, may be caused by the silica functional layer and may assist in uniform CNT growth. It can be seen that the nanocatalyst particle size in each case correlates with the CNT diameters observed by SEM and TEM and further validates the hypothesis that CNT size is largely governed by catalyst particles.

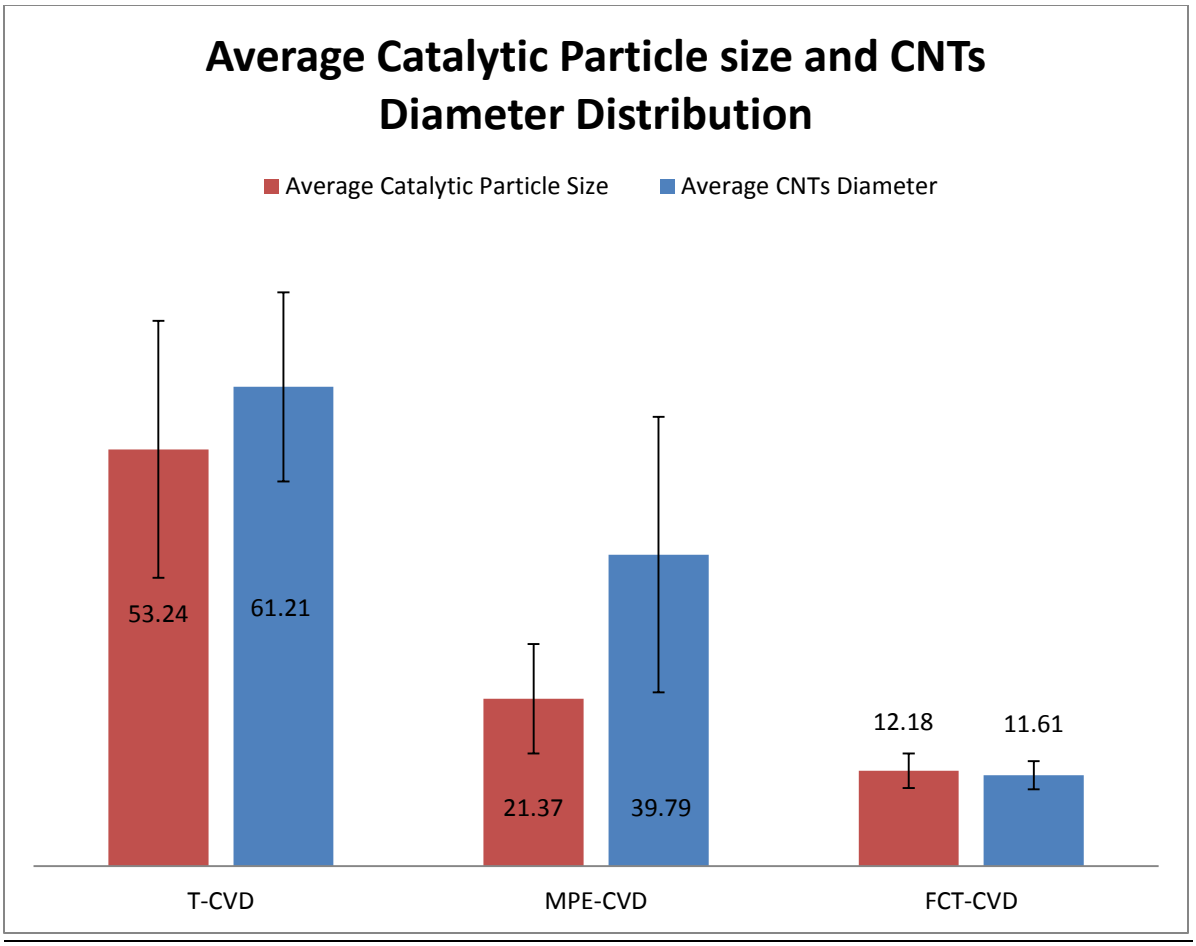

Figure 6: Particle size and CNTs tube diameter distribution chart.

3.4 Raman Spectrograph results:

Raman spectroscopy was performed on samples produced by the different growth methods. The results are presented in Figure 7. According to Handbook of Raman Spectroscopy and Dresselhaus, et al., Raman spectroscopy can be used as a guide to describe different carbon structures, such as diamond-like carbon which has C-C sp^3 bonding, graphitic carbon which has sp^2 bonding, and glassy/amorphous carbon, which has C-H and disordered mixed bonds [25,30,31]. The peaks found around 1350-1365 cm^{-1} are called D-peaks, resulting from the disorderly network of sp^2 and sp^3 carbon clusters, whereas the peaks found around 1580-1620

cm^{-1} are called G-peaks as a result of graphite, and finally the peak found at 1332 cm^{-1} is the diamond peak [30–32]. The most interesting finding from our experiment concerned the calculated intensity of the D-peak to G-peak ratios (I_D/I_G). This ratio matched the CNT morphology in terms of defect appearance in the SEM. The I_D/I_G ratios are given as follows: T-CVD = 0.30; MPE-CVD = 1.94; FCT-CVD = 0.84. Note that the T-CVD has the lowest I_D/I_G ratio; its SEM images indicated that this tube structure looks smoothest. In contrast, the I_D/I_G for MPE-CVD is the highest and its SEM images indicated that the tube structure appears damaged and full of defects. Earlier, we stated that hydrogen may etch the CNT and introduce defect sites that can raises the intensity of the D-peak. Another possibility is that when CNT is introduced to a hydrogen rich environment, the hydrogen causes C-H bonding, or transforms some CNTs into diamond or disordered carbon [27,33]. If this is the case, it explains why the disordered bonding peak, the D-peak, is much higher in the MPE-CVD sample.

Since the CNTs were grown on diamond substrates, one might suggest that the high intensity of D-peak resulted from signals coming from the diamond substrate underneath. However, the recorded D-peak intensity lies around (1354 cm^{-1}), whereas known diamond D-peaks are detected at (1332 cm^{-1}), indicating that the peak signal did not result from the diamond substrate. For confirmation, a razor blade was used to scrape away the CNTs from a sample and expose the diamond substrate underneath. The Raman spectra taken from the exposed diamond surface has a peak intensity at (1338 cm^{-1}), which closely matches the published Raman peak for diamond (1332 cm^{-1}). This additional test further indicates that the (1354 cm^{-1}) peak is indeed the D-peak from disordered CNT and not from the diamond substrate.

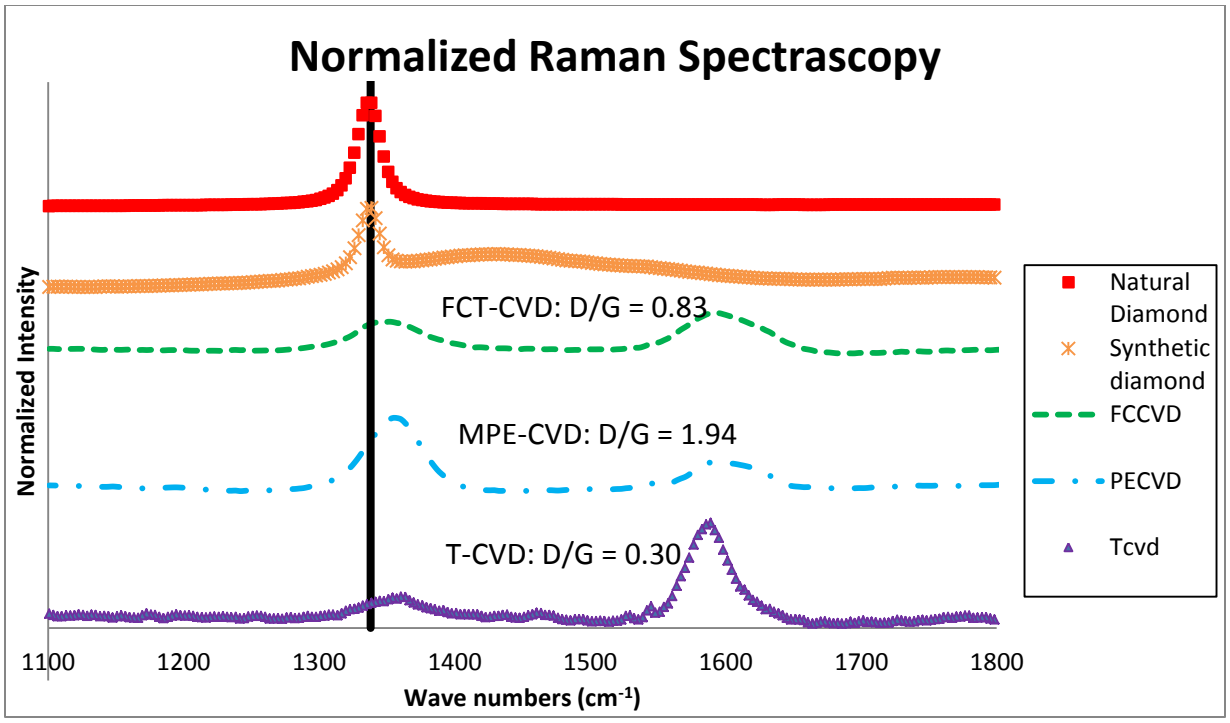

Figure 7: Raman spectroscopy signals for natural diamond, synthetic diamond, and CNTs from three CVD methods.

3.5 Sonication Results:

If the sample was used in a commercial device, it would be important to know if the CNTs had the strength to stay intact within the substrate. The sonication test was used as a qualitative comparison of the forces needed to detach CNT from the substrate [34,35]. SEM images were taken before and after sonication tests as shown in Figure 8a T-CVD, Figure 8b MPE-CVD, and Figure 8c FCT-CVD. There were no detectable differences seen in the before and after images from SEM. The optical images before the sonication test for the three growth methods were similar and are represented by Figure 8d. The optical images after the sonication test were similar for T-CVD and FCT-CVD also represented by Figure 8d. The MPE-CVD after sonication sample was different as shown in Figure 8e. The post sonication SEM images of

MPE-CVD sample indicated that CNTs were present on the surface, while optical images highlighted the exposed diamond substrate on the corners of the sample. This indicates detachment of CNTs at corners of this sample, implying that bonding between CNTs and substrate may be the weakest in this method. It must be noted that because of the extremely high length/diameter ratio of the nanotubes, agitation in an ultrasonic bath produces concentrated stresses at the root of the CNT. Survival under these conditions may indicate these materials will be robust in many service conditions. Among the three samples, MPE-CVD specimen may be the weakest.

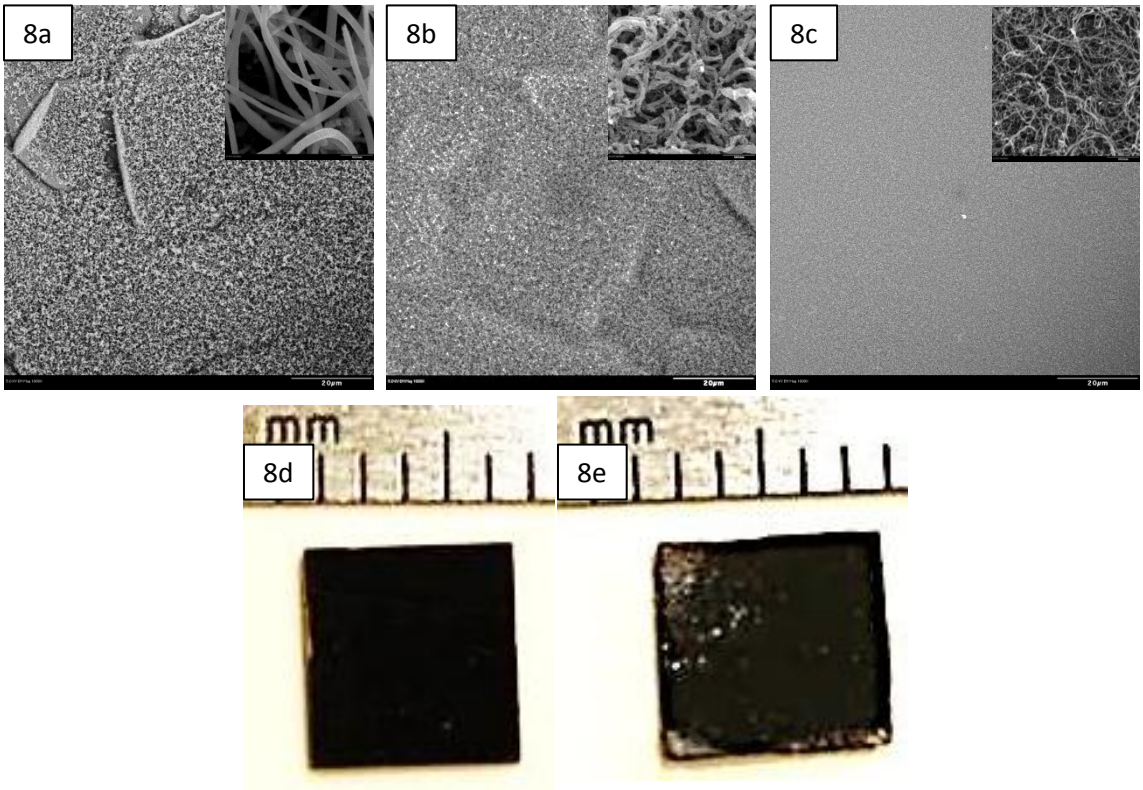

Figure 8: 8a, 8b, and 8c are SEM images representing before and after sonication test. 8d and 8e are optical images. 8a: T - CVD. 8b: MPE - CVD. 8c: FCT - CVD. 8d: represents before and after sonication tests for T - CVD and FCT - CVD, and only before sonication test for MPE - CVD. 8e: MPE-CVD after sonication test.

3.6 Overall comparison:

It is seen that very different types of CNT layers can be grown on diamond film by different techniques. It must be noted that T-CVD and MPE-CVD are multistep processes that separate the catalyst deposition step from the CNT growth step. The catalytic particles in the T-CVD growth are found to be the largest of the three types of growth. These particles were found to reside at the interface with minimal migration into the CNT layer. The resulting CNT structures were found to be the smoothest with largest tube diameters of all three growth types. This smooth structure may be useful for electronic and thermal applications that require minimal defects.

The SEM images show the CNTs that resulted from the MPE-CVD method contains kinks and defects on the individual tubes. The defects may be the result of hydrogen plasma and excess hydrogen in the chamber. The excess hydrogen can etch the surface of CNTs as it grows, which results in a defected surface. The hydrogen plasma may also provide excess energy that inadvertently promotes catalyst migration. If this migration occurs during CNT growth, it may be another underlying reason as to why those CNT structures are kinked. It can be proposed that as the CNTs are growing with the migrating catalytic particles, a straight path for growth was not provided, which resulted in a kinked-type growth. Therefore, this approach which is suitable for large area growth will be useful only in situations where defective and kinked CNTs are acceptable. It would be interesting to determine if the defective CNTs grown under energetic conditions are more reactive then their smoother counterparts. Another noticeable difference provided by the MPE-CVD method is that it has the weakest bonding with the substrate compared to the other two methods. Images from the three growth methods were compared after the sonication test. The images from the sonication test shows the corners of the diamond substrate were exposed after the test, which is not seen in the other samples. The benefit of using

FCT-CVD is that it is a one step process where catalyst and carbon source are introduced together. The resulting CNTs grown by this process had the smallest diameter, averaging 12 nm, with uniform and dense growth patterns. While this may be a very suitable approach in many applications, the disadvantage is the possibility of excess iron particles arising from continuous catalyst deposition. This may be mitigated by modifying the process to cut off ferrocene during the latter part of CNT growth.

Since each method has its unique advantages and disadvantages, these studies indicate that the selection of the CNT growth method is heavily influenced by the intended application.

4. Conclusions

In this research, we have compared the growth of CNTs forests on synthetic diamond substrates using three different CVD growth methods. The CNTs were characterized using electron microscope imaging (SEM and TEM), elemental analysis (EDS), Raman spectroscopy and the sonication test. The SEM and TEM images indicated each method produces CNTs with distinctly different diameter and morphology. Raman spectroscopic analysis suggested T-CVD had the lowest disordered carbon to graphite intensity ratio of 0.3 followed by FCT-CVD of 0.83 and highest by MPE-CVD of 1.94. T-CVD also produces large diameter CNTs that are otherwise clean, with minimal tubular defects or additional catalytic contaminants. MPE-CVD is sometimes the preferred method for larger scaled applications; however the excess hydrogen plasma energy during growth may cause migrations of catalytic particles, surface etching, and defective CNTs that may be detrimental to precision applications. MPE-CVD has the highest probability for catalytic mobility, the most defective CNTs structure morphology, and weakest interfacial bonding strength. FCT-CVD has the advantage of being a one-step CNT growth

method that does not need a separate catalyst deposition step, yet produces dense uniform CNTs. This technique provided the finest CNT diameter, and intermediate diamond/graphite ratio in the Raman signal. This method does produce some excess metal particles due to continuous catalyst nucleation. However, this issue can be easily addressed in future if needed, by stopping the catalytic source after a certain growth time. Finally, this study indicates that there is a clear correlation between the size of catalyst particle and the CNT diameters.

5. Acknowledgements:

The authors of the paper would like to thank the funding support of Air Force Office of Scientific Research, Air Force Research Laboratory Propulsion Directorate, Wright State University and Ohio Board of Regents. The authors would like to acknowledge Dr. Robert Wheeler for his guidance on TEM and EDS.

References:

[1] Meyyappan M. Carbon Nanotubes: Science and Applications. Boca Ratton: CRC Press; 2004.

[2] Iijima S. Nature 1991;354:56.

[3] Saito, R., Fujita, M., Dresselhaus, G., Dresselhaus MS. Applied Physics Letters 1992;60:2204.

[4] Calvert P. Nature 1992;357:356.

[5] Novikov NV, Dub SN. Diamond and Related Materials 1996;5:1026.

[6] Kidalov S V., Shakhov FM. Materials 2009;2:2467.

[7] Lee CJ, Lyu SC, Cho YR, Lee JH, Cho KI. Chemical Physics Letters 2001;341:245.

[8] Thostenson ET, Ren Z, Chou T-W. Composites Science and Technology 2001;61:1899.

[9] Tumilty N, Kasharina L, Prokhoda T, Sinelnikov B, Jackman RB. Carbon 2010;48:3027.

[10] Varanasi C, Petry J, Brunke L, Yang BT, Lanter W, Burke J, Wang H, Bulmer JS, Scofield J, Barnes PN. Carbon 2010;48:2442.

[11] Takagi D, Kobayashi Y, Homma Y. Journal of the American Chemical Society 2009;131:6922.

[12] Li Y, Kim W, Zhang Y, Rolandi M, Wang D, Dai H. The Journal of Physical Chemistry B 2001;105:11424.

[13] Sehested J, Hansen PL, Helveg S, Lo C, Clausen BS, Rostrup-nielsen JR, Abild-pedersen F. Nature 2004;427:427.

[14] Baker RTK, Barber MA, Harris PS, Feates FS, Waite RJ. Journal of Catalysis 1972;26:51.

[15] Wirth CT, Hofmann S, Robertson J. Diamond and Related Materials 2009;18:940.

[16] Raty J-Y, Gygi F, Galli G. Physical Review Letters 2005;95.

[17] Hofmann S, Csányi G, Ferrari A, Payne M, Robertson J. Physical Review Letters 2005;95.

[18] Koziol K, Boskovic BO, Yahya N. Carbon and Oxide Nanostructures: Synthesis, Characterisation and Applications. Columbia: Henry Dickens & Co.; 2011.

[19] Choi YC, Bae DJ, Lee YH, Lee BS, Park G-S, Choi WB, Lee NS, Kim JM. Journal of Vacuum Science & Technology A: Vacuum, Surfaces, and Films 2000;18:1864.

[20] Teo, Kenneth B K., Singh, C., Chhowalla, M., Milne W. Encyclopedia of Nanoscience and Nanotechnology 2003;X:1.

[21] Fernandes a. JS, Pinto M, Neto M a., Oliveira FJ, Silva RF, Costa FM. Diamond and Related Materials 2009;18:160.

[22] Cao A, Ajayan PM, Ramanath G, Baskaran R, Turner K. Applied Physics Letters 2004;84:109.

[23] Mukhopadhyay SM, Karumuri A, Barney IT. Journal of Physics D: Applied Physics 2009;42.

[24] Mukhopadhyay S, Joshi P, Pulikollu R. Tsinghua Science & Technology 2005;10:709.

[25] Lauer JL. Handbook of Raman Spectroscopy from the Research Laboratory to the Process Line, first ed. West Yorkshire: Marcel Dekker, Inc; 2001.

[26] Homma Y, Kobayashi Y, Ogino T, Takagi D, Ito R, Jung YJ, Ajayan PM. The Journal of Physical Chemistry B 2003;107:12161.

[27] Behr MJ, Gaulding EA, Mkhoyan KA, Aydil ES. Journal of Vacuum Science & Technology B: Microelectronics and Nanometer Structures 2010;28:1187.

[28] Sun LT, Gong JL, Zhu ZY, Zhu DZ, He SX, Wang ZX, Chen Y, Hu G. Applied Physics Letters 2004;84:2901.

[29] Yang Q, Yang S, Xiao C, Hirose A. Materials Letters 2007;61:2208.

[30] Dresselhaus MS, Dresselhaus G, Saito R, Jorio A. Physics Reports 2005;409:47.

[31] Dresselhaus MS, Jorio a, Souza Filho a G, Saito R. Philosophical transactions Series A, Mathematical, physical, and engineering sciences 2010;368:5355.

[32] O'brien LC, Kubicek RL, O'brien JJ. Highlights 1994;71:759.

[33] Zhang G, Qi P, Wang X, Lu Y, Mann D, Li X, Dai H. Journal of the American Chemical Society 2006;128:6026.

[34] Zhang Q, Liu J, Sager R, Dai L, Baur J. Composites Science and Technology 2009;69:594.

[35] Riccardis MF De, Carbone D, Makris TD, Giorgi R, Lisi N, Salernitano E. Carbon 2006;44:671.